2021 American Control Conference (ACC)
New Orleans, USA, May 25-28, 2021

Robustness of variance suppression in channel flows with imperfect transverse wall oscillations

Dhanushki Hewawaduge, Tyler Summers, and Armin Zare

***Abstract*— Transverse wall oscillations are a sensor-free control strategy that can suppress kinetic energy and reduce skin-friction drag in wall-bounded shear flows. However, the success of wall oscillations is tied to the appropriate selection of their amplitude and frequency. We evaluate the robust performance of this flow control strategy to imperfections in the amplitude and phase of oscillations. These imperfections, which are modeled as stochastic parametric uncertainties, appear as multiplicative uncertainties in the linearized dynamics. We adopt an input-output approach to analyze the mean-square stability and frequency response of the flow subject to additive and multiplicative sources of uncertainty and provide a computationally efficient method for computing the energy spectrum of velocity fluctuations around the uncertain base state.**

***Index Terms*— Sensor-free flow control, stability analysis, stochastically forced Navier-Stokes, structured uncertainty, time-periodic systems, vibrational control.**

I. Introduction

Carefully designed transverse wall oscillations have been shown to reduce the receptivity of wall-bounded flows to exogenous disturbances, suppress energy of velocity fluctuations, and reduce skin-friction drag by 40%. However, experimental [1], [2], numerical [3], [4], and theoretical studies [5]–[7] have demonstrated that the efficacy of this flow control strategy depends on a critical selection of design parameters, e.g., amplitude and frequency [6]. This motivates the development of a complementary framework for analyzing the robust performance of such vibrational control strategies that are prone to parametric uncertainties resulting from implementation and modeling imperfections.

The linearized Navier-Stokes (NS) equations have been shown to capture structural and statistical features of transitional [8]–[11] and turbulent [12]–[15] shear flows. This success has paved the way for the model-based design of passive flow control strategies for suppressing turbulence or reducing drag [6], [7], [16], [17]. In these studies, additive stochastic excitation is used to model the effect of background disturbances or to obtain the statistical response of the linearized dynamics. On the other hand, uncertainty in system parameters and coefficients enter the linearized dynamics multiplicatively and in a structured manner. For a small number of deterministic and set-valued uncertainties, the structured singular value can be used to provide a robust stability theory for uncertain dynamics [18]. However, implementation deficiencies often results in unpredictable time-varying parametric variations. Herein, we model time-varying parametric variations in the amplitude and phase of wall oscillations as white-in-time stochastic signals that enter the linearized NS equations as multiplicative uncertainties.

In the absence of stochastic parametric uncertainties, the linearized dynamics of channel flow over harmonic wall oscillations are time-periodic. In this case, the $\mathcal{H}_2$ norm of the Linear Time-Periodic (LTP) system can be expressed in terms of the solution to the harmonic Lyapunov equation [19] and perturbation analysis can be used to solve such equations efficiently [20]. Parametric uncertainties introduce multiplicative sources of stochasticity into the coefficients of the otherwise LTP system resulting in Stochastic Differential Equations (SDEs) whose treatment requires an appropriate stochastic calculus. We rewrite the SDEs as a feedback interconnection of LTP dynamics and structured stochastic uncertainties and build on the developments of [21] to provide specialized conditions for the Mean-Square Stability (MSS) of the uncertain dynamics. The $\mathcal{H}_2$ norm of the SDEs that quantifies the receptivity of fluctuations to additive and multiplicative sources of excitation can be expressed in terms of the solution to a generalized Lyapunov equation [22]. We show how perturbation analysis can be used to obtain the solution of this generalized Lyapunov equation from a set of ordered smaller-size Lyapunov equations.

A. Problem formulation

Three-dimensional pressure-driven channel flow of incompressible Newtonian fluid is governed by the NS equations

$$\begin{aligned} \mathbf{u}_t &= -(\mathbf{u}\cdot\nabla)\,\mathbf{u} - \nabla P + \frac{1}{R}\,\Delta\mathbf{u} \\ 0 &= \nabla\cdot\mathbf{u} \end{aligned} \tag{1}$$

where $\mathbf{u}$ and $\mathbf{u}_t$ are the velocity vector and its time derivative, P is pressure, ∇ is the gradient, $\Delta = \nabla\cdot\nabla$ is the Laplacian, and $R = \bar{U}h/\nu$ is the Reynolds number defined in terms of the centerline velocity $\bar{U}$, channel half-height h, and kinematic viscosity ν. Figure 1(a) shows the geometry of a channel for which the streamwise, wall-normal, and spanwise coordinates are represented by x, y, and z, respectively.

In addition to the driving streamwise pressure gradient P_x, we assume the flow to be subject to lower-wall transverse sinusoidal oscillations of amplitude α and frequency ω_t that take the form $2\alpha\,(1+\gamma_\alpha)\sin(\omega_t\,t + \gamma_\theta)$; see Fig. 1(b). Here, the amplitude of wall oscillations is multiplied by 2 for convenience of algebraic manipulations, and $\gamma_\alpha(t)$ and $\gamma_\theta(t)$ represent independent sources of white-in-time stochastic

Dhanushki Hewawaduge, Tyler Summers, and Armin Zare are with the Department of Mechanical Engineering, University of Texas at Dallas, Richardson, TX 75080, USA. E-mails: {dhanushki.hewawaduge, tyler.summers, armin.zare}@utdallas.edu.

978-1-6654-4197-1/$31.00 ©2021 AACC

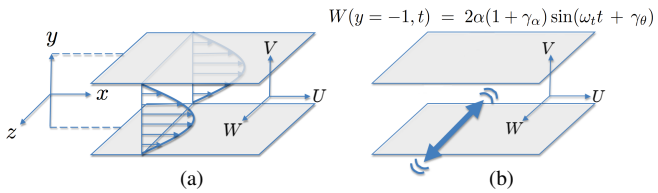

Fig. 1. (a) Pressure driven channel flow; and (b) channel flow subject to transverse wall oscillations with amplitude and phase imperfections.

uncertainty with mean and variance given by $\{\mu_\alpha, \sigma_\alpha^2\}$ and $\{\mu_\theta, \sigma_\theta^2\}$, respectively. These parametric uncertainties model imperfections in the amplitude and phase of oscillations and effectively result in random lower-wall oscillations.

While the streamwise and wall-normal components of the three-dimensional velocity field satisfy no-slip/no-penetration boundary conditions at both walls, the spanwise component adopts a harmonic boundary condition at the lower-wall that is contaminated with stochastic parameters γ_α and γ_θ. Solving the NS equations subject to the described boundary conditions with different realizations of uncertain parameters is computationally expensive. This motivates the development of a framework for studying the influence of structured stochastic uncertainty on the stability and receptivity of NS equations using low-complexity models.

B. Paper outline

In Section II, we determine the base velocity of channel flow over transverse wall oscillations with amplitude/phase uncertainty, and obtain the linearized NS equations. In Section III, we rewrite the linearized dynamics as a feedback interconnection between nominal dynamics and sources of stochastic uncertainty, and use this representation to provide MSS conditions. In Section IV, we exploit the time-periodicity of the nominal dynamics to characterize the frequency response, and provide a computationally efficient method for determining the energy spectrum of velocity fluctuations. In Section V, we examine the MSS of channel flow over random wall oscillations and discuss the influence of parametric uncertainty on suppressing the energy of velocity fluctuations. We provide concluding remarks in Section VI.

II. Dynamics of velocity fluctuations

In the presence of the transverse wall oscillations described in Section I-A, the base flow $\bar{\mathbf{u}} = [\,U \;\; V \;\; W\,]^T$ can be obtained by solving Eqs. (1) in steady-state subject to

$$\begin{aligned} U(\pm1) \;&=\; V(\pm1) \;=\; V_y(\pm1) \;=\; W(1) \;=\; 0 \\ W(-1) \;&=\; 2\,\alpha\,(1+\gamma_\alpha)\sin(\omega_t t+\gamma_\theta). \end{aligned} \tag{2}$$

Due to these boundary conditions, the equations that govern the dynamics of the base flow can be simplified into a pair of decoupled partial differential equations

$$\begin{aligned} 0 \;&=\; -\bar{P}_x \;+\; (1/R)U_{yy} \\ W_t \;&=\; (1/R)W_{yy} \end{aligned} \tag{3}$$

where $\bar{P}_x = -2/R$ denotes the nominal pressure gradient in Poiseuille flow. The steady-state solution to (2) and (3) is given by $\bar{\mathbf{u}} := [\,U(y) \;\; 0 \;\; W(y,t)\,]^T$, with

$$U(y) \;=\; 1 - y^2 \tag{4a}$$

$$\begin{aligned} W(y,t) \;=\; \alpha\,\big[&(1+\gamma_{+1})\,W_{+1}(y)\,\mathrm{e}^{\mathrm{i}\omega_t t} \\ &+\; (1+\gamma_{-1})\,W_{-1}(y)\,\mathrm{e}^{-\mathrm{i}\omega_t t}\big]. \end{aligned} \tag{4b}$$

Here, $\gamma_{\pm1} := (1+\gamma_\alpha)\,\mathrm{e}^{\pm\mathrm{i}\gamma_\theta} - 1$ are white-in-time stochastic uncertainties that capture the effects of γ_α and γ_θ on the base state with means and variances [23, Appendix B]

$$\begin{aligned} \mu_{\pm1} \;&=\; \mathbf{E}[\gamma_{\pm1}] \;=\; (1+\mu_\alpha)\,\mathrm{e}^{\pm\mathrm{i}\mu_\theta + \sigma_\theta^2/2} \;-\; 1, \\ \sigma_{\pm1}^2 \;&=\; \mathrm{e}^{\pm2\,\mathrm{i}\mu_\theta + \sigma_\theta^2}\left(\sigma_\alpha^2\mathrm{e}^{\sigma_\theta^2} \;+\; (1+\mu_\alpha)^2(\mathrm{e}^{\sigma_\theta^2} \;-\; 1)\right). \end{aligned}$$

Furthermore, $W_{\pm1}(y)$ are solutions to the system of ordinary differential equations

$$\begin{aligned} W_{+1}''(y) \;&=\; \mathrm{i}\omega_t R\,W_{+1}(y), \quad W_{-1}''(y) \;=\; -\mathrm{i}\omega_t R\,W_{-1}(y) \\ W_{+1}(1) \;&=\; W_{-1}(1) \;=\; 0, \quad W_{\pm1}(-1) \;=\; \mp\mathrm{i} \end{aligned} \tag{5}$$

where $W_{\pm1}''(y)$ denote second derivatives with respect to y; see [23, Appendix C] for a solution to Eqs. (5). In Eq. (4b), $\gamma_\alpha = \gamma_\theta = 0$ yields the nominal velocity

$$\bar{W}(y,t) \;=\; \alpha\,\big[W_1(y)\mathrm{e}^{\mathrm{i}\omega_t t} \;+\; W_{-1}(y)\mathrm{e}^{-\mathrm{i}\omega_t t}\big]. \tag{6}$$

The dynamics of velocity $\mathbf{v} = [\,u \;\; v \;\; w\,]^T$ and pressure p fluctuations around the base flow $\bar{\mathbf{u}} = [\,U(y) \;\; 0 \;\; W(y,t)\,]^T$ and $\bar{P}_x$ are governed by the linearized NS equations,

$$\begin{aligned} \mathbf{v}_t \;&=\; -\,(\bar{\mathbf{u}}\cdot\nabla)\,\mathbf{v} - (\mathbf{v}\cdot\nabla)\,\bar{\mathbf{u}} - \nabla p + \frac{1}{R}\,\Delta\mathbf{v} \;+\; \mathbf{f} \\ 0 \;&=\; \nabla\cdot\mathbf{v} \end{aligned} \tag{7}$$

Here, $\mathbf{f}$ is a zero-mean white-in-time stochastic forcing that represents three-dimensional exogenous excitations to the fluctuation dynamics. The uncertain base flow $\bar{\mathbf{u}}$ enters the linearized Eqs. (7) as a coefficient that multiplies the vector of velocity fluctuations $\mathbf{v}$. While $\bar{\mathbf{u}}$ includes multiplicative sources of uncertainty $\gamma_{\pm1}$, it remains constant in x and z and includes temporal harmonics of period $T = 2\pi/\omega_t$. Elimination of pressure and application of the Fourier transform in the spatially invariant directions x and z brings Eqs. (7) into the evolution form

$$\begin{aligned} \boldsymbol{\psi}_t(y,\mathbf{k},t) \;&=\; A(\mathbf{k},t)\,\boldsymbol{\psi}(y,\mathbf{k},t) \;+\; B(\mathbf{k})\mathbf{f}(y,\mathbf{k},t) \\ \mathbf{v}(y,\mathbf{k},t) \;&=\; C(\mathbf{k})\,\boldsymbol{\psi}(y,\mathbf{k},t) \end{aligned} \tag{8}$$

where the state $\boldsymbol{\psi} := [\,v \;\; \eta\,]^T$ contains the wall-normal velocity v and vorticity $\eta = \partial_z u - \partial_x w$, and $\mathbf{k} = [\,k_x \;\; k_z\,]^T$ is the vector of streamwise and spanwise wavenumbers. Equations (8) are SDEs that involve both additive and multiplicative sources of stochastic uncertainty with operators A, B, and C given in [6, Eq. (6)].

Following the structure of $\bar{\mathbf{u}}$, the operator-valued matrix A in the evolution model (8) can be decomposed as

$$\begin{aligned} A(\mathbf{k},t) \;=\; \bar{A}(\mathbf{k}) \;+\; \alpha\,\big[&\gamma_{+1}A_{+1}(\mathbf{k})\,\mathrm{e}^{\mathrm{i}\omega_t t} \\ &+\gamma_{-1}A_{-1}(\mathbf{k})\,\mathrm{e}^{-\mathrm{i}\omega_t t}\big] \end{aligned} \tag{9}$$

where

$$\bar{A}(\mathbf{k},t) \;=\; A_0(\mathbf{k}) \;+\; \alpha\left((1\;+\;\mu_{+1})\,A_1(\mathbf{k})\,\mathrm{e}^{\mathrm{i}\omega_t t} \;+\; (1\;+\;\mu_{-1})\,A_{-1}(\mathbf{k})\,\mathrm{e}^{-\mathrm{i}\omega_t t}\right) \tag{10}$$

and expressions for A_0, A_1 and A_{-1} are provided in [23, Appendix D]. Here, we have explicitly accounted for the dynamic drift resulting from the mean values of uncertainties $\gamma_\pm$, i.e., $\mu_{\pm1}$, by including a constant modification to the coefficients of the otherwise purely time-periodic deterministic dynamics $\bar{A}$. In the remainder of the paper, we will consider sources of multiplicative uncertainty $\gamma_{\pm1}$ to have zero mean.

III. Input-output formulation and MSS conditions

The evolution of $\boldsymbol{\psi}$ in SDE (8) is affected by the presence of both stochastic parametric uncertainties and additive forcing. While there is no ambiguity in the treatment of additive noise in continuous-time systems, multiplicative noise is not generally well-defined and its treatment calls for the adoption of a suitable stochastic calculus (e.g., Itō [24] or Stratonovich [25]). In this section, we provide an appropriate interpretation for the multiplicative uncertainty, extract these sources using a linear fractional transformation, and establish an input-output relation between stochastic sources and the output velocity fluctuations of system (8). Building on this representation, we examine conditions for MSS in the presence of multiplicative stochastic uncertainty.

A. Stochastic feedback interconnection

In input-output form, SDE (8) can be rewritten as

$$\begin{bmatrix}\mathbf{v}(\mathbf{k},t)\\ \mathbf{z}(\mathbf{k},t)\end{bmatrix} \;=\; \int_0^t M(\mathbf{k},t\;-\;\tau)\begin{bmatrix}\mathbf{f}(\mathbf{k},\tau)\\ \mathbf{r}(\mathbf{k},\tau)\end{bmatrix}\mathrm{d}\tau$$

$$\mathbf{r}(\mathbf{k},t) \;=\; \mathcal{D}(\gamma(t))\,\mathbf{z}(\mathbf{k},t) \tag{11}$$

which extracts the role of multiplicative uncertainties by rearranging the dynamics as a feedback connection between the nominal dynamics and the structured uncertainty $\mathcal{D}(\gamma(t)) := \mathrm{diag}\{\gamma_{-1}(t)I, \gamma_1(t)I\}$. In (11), M denotes the finite-dimensional approximation to the impulse response operator, $\mathbf{v}$ is the output velocity vector, and $\mathbf{z}$ is computed from the state $\boldsymbol{\psi}$. Moreover, exogenous stochastic input $\mathbf{f}$, uncertain feedback signal $\mathbf{r}$, and sources of parametric uncertainty γ_i are white processes that are defined as derivatives of Wiener processes (or Brownian motion) [26], i.e.,

$$\gamma_i(t) := \frac{\mathrm{d}\tilde{\gamma}_i(t)}{\mathrm{d}t};\;\; \mathbf{f}(\mathbf{k},t) := \frac{\mathrm{d}\tilde{\mathbf{f}}(\mathbf{k},t)}{\mathrm{d}t};\;\; \mathbf{r}(\mathbf{k},t) := \frac{\mathrm{d}\tilde{\mathbf{r}}(\mathbf{k},t)}{\mathrm{d}t}.$$

Here, $\tilde{\gamma}_i(t)$ are zero-mean Wiener processes with variance σ_i^2 and $\tilde{\mathbf{f}}$ is a zero-mean vector-valued Wiener process with instantaneous covariance $\mathbf{E}(\tilde{\mathbf{f}}(\mathbf{k},t)\,\tilde{\mathbf{f}}^*(\mathbf{k},t)) = \Omega(\mathbf{k})t$, in which $\Omega(\mathbf{k}) = \Omega^*(\mathbf{k}) \succeq 0$ is the spatial covariance matrix. We assume that $\tilde{\gamma}_i$ and $\tilde{\mathbf{f}}$ are uncorrelated for all time, adopt the Itō interpretation, and assume that $\mathbf{r}(t)$ has temporally independent increments [21], i.e., its differentials $(\mathrm{d}\mathbf{r}(t_1), \mathrm{d}\mathbf{r}(t_2))$ are independent for $t_1 \neq t_2$. Given this mathematical interpretation, the differential form of Eqs. (11) are given by

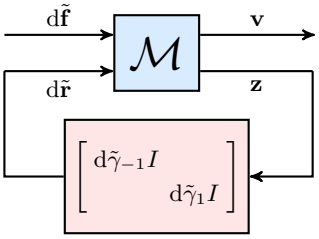

Fig. 2. Linear fractional transformation of an LTI system subject to both additive and multiplicative stochastic disturbances (Eqs. (13)). Here, $\mathrm{d}\tilde{\mathbf{f}}$ and $\mathrm{d}\tilde{\gamma}_i$ represent differentials of Wiener processes that model additive and multiplicative sources of stochastic uncertainty, respectively.

$$\begin{bmatrix}\mathbf{v}(\mathbf{k},t)\\ \mathbf{z}(\mathbf{k},t)\end{bmatrix} \;=\; \int_0^t M(\mathbf{k},t\;-\;\tau)\begin{bmatrix}\mathrm{d}\tilde{\mathbf{f}}(\mathbf{k},\tau)\\ \mathrm{d}\tilde{\mathbf{r}}(\mathbf{k},\tau)\end{bmatrix}$$

$$\mathrm{d}\tilde{\mathbf{r}}(\mathbf{k},t) \;=\; \mathcal{D}(\mathrm{d}\tilde{\gamma}(t))\,\mathbf{z}(\mathbf{k},t) \tag{12}$$

and are described by the block diagram in Fig. 2. A corresponding state-space representation is given by

$$\mathcal{M}:\begin{cases}\mathrm{d}\boldsymbol{\psi}(t) \;=\; \bar{A}(t)\,\boldsymbol{\psi}(t)\mathrm{d}t \;+\; B_0(t)\,\mathrm{d}\tilde{\mathbf{r}}(t) \;+\; B\,\mathrm{d}\tilde{\mathbf{f}}(t)\\ \mathbf{z}(t) \;=\; C_0(t)\,\boldsymbol{\psi}(t)\\ \mathbf{v}(t) \;=\; C\,\boldsymbol{\psi}(t)\end{cases}$$

$$\mathrm{d}\tilde{\mathbf{r}}(t) \;=\; \mathcal{D}(\mathrm{d}\tilde{\gamma}(t))\,\mathbf{z}(t) \tag{13}$$

where the dependence of vectors and matrices on the horizontal wavenumber pair $\mathbf{k}$ has been omitted for brevity, $\bar{A}$ is the nominal time-periodic dynamic matrix (Eq. (10)), and

$$B_0 := \begin{bmatrix} I & I \end{bmatrix}, \quad C_0 := \begin{bmatrix} A_{-1}\mathrm{e}^{-\mathrm{i}\omega_t t} \\ A_{+1}\mathrm{e}^{+\mathrm{i}\omega_t t} \end{bmatrix}.$$

B. Mean-square stability conditions

Mean-square stability is a strong form of stability that implies stability of the mean and convergence of all trajectories of the stochastic dynamical system (in the absence of persistent exogenous excitation) to zero with probability one [27], [28]. The MSS of the causal LTI system (13) certifies that for all differential inputs, $[\,\mathrm{d}\tilde{\mathbf{f}}\;\;\mathrm{d}\tilde{\mathbf{r}}\,]^T$, with independent increments and uniformly bounded variance, the output process, $[\,\mathbf{v}\;\;\mathbf{z}\,]^T$, has a uniformly bounded variance; see, e.g., [29]. Following [21, Theorem 2], the necessary and sufficient conditions for the MSS of (13) are: (i) $\bar{A}$ is Hurwitz; and (ii) the spectral radius of the loop gain operator

$$\mathbb{L}(\bar{\mathbf{R}}) \;:=\; \Gamma \circ \left(\int_0^\infty M_{22}(\tau)\,\bar{\mathbf{R}}\,M_{22}^\dagger(\tau)\mathrm{d}\tau\right)$$

is strictly less than 1, i.e., $\rho(\mathbb{L}) < 1$. Here, Γ is the mutual correlation matrix of $\tilde{\gamma}_i$, i.e., $\Gamma := \mathbf{E}(\tilde{\gamma}_i(t)\,\tilde{\gamma}_j^*(t))$, $\circ$ is the Hadamard product, M_{22} is the impulse response of the subsystem $\mathcal{M}_{22} : \mathrm{d}\tilde{\mathbf{r}} \to \mathbf{z}$, which is given by

$$M_{22}(\mathbf{k},t) \;=\; C_0(\mathbf{k})\,\mathrm{e}^{\bar{A}(\mathbf{k},t)t}\,B_0(\mathbf{k})$$

and $\dagger$ denotes the adjoint of an operator, which is determined with respect to the inner products corresponding to the

underlying function spaces; see, e.g., [10].

The loop gain operator propagates the steady-state covariance of $\mathrm{d}\tilde{\mathbf{r}}$ denoted by $\bar{\mathbf{R}}$ through the feedback configuration in Fig. 2. Equivalently, we have

$$\mathbb{L}(\bar{\mathbf{R}}) \;=\; \Gamma \circ (C_0\, X\, C_0^\dagger)$$

where X is the solution to the algebraic Lyapunov equation

$$\bar{A}\, X \;+\; X\, \bar{A}^\dagger \;=\; -B_0\, \bar{\mathbf{R}}\, B_0^\dagger.$$

The spectral radius of $\mathbb{L}$ can be numerically calculated using the power iteration algorithm in [23, Section III.B].

IV. Frequency response of uncertain dynamics

We build on the input-output representation provided in Section III and exploit the time-periodicity of the nominal dynamics to characterize the frequency response of the system subject to additive and multiplicative uncertainties. We show that the energy spectrum of velocity fluctuations can be obtained from the solution of a generalized Lyapunov equation. For small-amplitude wall oscillations, we employ a perturbation analysis to achieve computational efficiency in solving the generalized Lyapunov equation.

A. Frequency response

The impulse response M in (12) corresponding to the state-space representation (13) takes the form

$$M(\mathbf{k},t) \;:=\; \begin{bmatrix} C(\mathbf{k}) \\ C_0(\mathbf{k}) \end{bmatrix} \mathrm{e}^{\bar{A}(\mathbf{k},t)t} \begin{bmatrix} B(\mathbf{k}) & B_0(\mathbf{k}) \end{bmatrix}$$

and inherits the time-periodicity of the nominal dynamics $\bar{A}$ (cf. (10)). Due to this time-periodicity, response vectors $\mathbf{v}$ and $\mathbf{z}$ of system (13) subject to stationary white processes $\mathrm{d}\tilde{\mathbf{f}}$ and $\mathrm{d}\tilde{\mathbf{r}}$ are cyclo-stationary processes [30], i.e., their statistical properties are periodic in time. As a result, the auto-correlation operator of $\boldsymbol{\psi}$ is given by

$$\begin{aligned} X(\mathbf{k},t) \;&=\; \mathbf{E}\left(\boldsymbol{\psi}(\mathbf{k},t)\boldsymbol{\psi}^*(\mathbf{k},t)\right) \qquad (14)\\ &=\; X_0(\mathbf{k}) \;+\; X_1(\mathbf{k})\,\mathrm{e}^{\mathrm{i}\omega_t t} \;+\; X_1^\dagger(\mathbf{k})\,\mathrm{e}^{-\mathrm{i}\omega_t t} \\ &\qquad +\; X_2(\mathbf{k})\,\mathrm{e}^{\mathrm{i}2\omega_t t} \;+\; X_2^\dagger(\mathbf{k})\,\mathrm{e}^{-\mathrm{i}2\omega_t t} \;+\; \ldots \end{aligned}$$

Moreover, the average effect of additive and multiplicative sources of excitation (over one period of wall oscillations T) is determined by the operator X_0, i.e.,

$$\frac{1}{T}\int_0^T X(\mathbf{k},t)\,\mathrm{d}t \;=\; X_0(\mathbf{k}) \qquad (15)$$

and the energy spectrum of velocity fluctuations is given by

$$E(\mathbf{k}) \;=\; \mathrm{trace}\left(X_0(\mathbf{k})\right). \qquad (16)$$

When $\mathbf{f}$ and γ_i are zero-mean white-in-time processes with covariance matrix Ω and variance σ_i^2, the frequency representation of the auto-correlation operator of state $\boldsymbol{\psi}$ is a self-adjoint bi-infinite block-Toeplitz operator of the form

$$\mathcal{X}(\mathbf{k}) \;=\; \mathrm{Toep}\left\{\ldots, X_2^\dagger, X_1^\dagger, \boxed{X_0}, X_1, X_2, \ldots\right\} \qquad (17)$$

that can be obtained from the generalized Lyapunov equation

$$\bar{\mathcal{F}}\,\mathcal{X} \;+\; \mathcal{X}\,\bar{\mathcal{F}}^\dagger \;+\; \sum_{i=\pm1} \sigma_i^2\, \mathcal{F}_i\, \mathcal{X}\, \mathcal{F}_i^\dagger \;=\; -\mathcal{B}\,\boldsymbol{\Omega}\,\mathcal{B}^\dagger \qquad (18a)$$

$$\bar{\mathcal{F}} \;:=\; \bar{\mathcal{A}} \;-\; \mathcal{E}(0) \qquad (18b)$$

$$\mathcal{F}_i \;:=\; \mathcal{A}_i \qquad (18c)$$

which is parameterized over wavenumber pairs $\mathbf{k}$. Here, $\mathcal{B}$, $\boldsymbol{\Omega}$, and $\mathcal{E}$ are bi-infinite block-diagonal operators,

$$\mathcal{B}(\mathbf{k}) \;:=\; \mathrm{diag}\left\{B(\mathbf{k})\right\}_{n\in\mathbb{Z}}$$

$$\boldsymbol{\Omega}(\mathbf{k}) \;:=\; \mathrm{diag}\left\{\Omega(\mathbf{k})\right\}_{n\in\mathbb{Z}}$$

$$\mathcal{E}(\theta) \;:=\; \mathrm{diag}\left\{\mathrm{i}\,(\theta \;+\; n\,\omega_t)\, I\right\}_{n\in\mathbb{Z}}$$

where $\theta \in [0, \omega_t)$ is the angular frequency, and $\bar{\mathcal{A}}$ and $\mathcal{A}_i$ are bi-infinite block-Toeplitz operators that represent the lifted variants of the nominal and uncertain components of the dynamics (cf. Eqs. (9) and (10)), respectively, i.e.,

$$\begin{aligned} \bar{\mathcal{A}} \;&:=\; \mathrm{Toep}\Big\{\ldots, 0, \alpha\,(1+\mu_1)A_1, \boxed{A_0}, \alpha\,(1+\mu_{-1})A_{-1}, 0, \ldots\Big\} \\ \mathcal{A}_1 \;&:=\; \mathrm{Toep}\Big\{\ldots, 0, \alpha\,A_1, \boxed{0}, 0, \ldots\Big\} \\ \mathcal{A}_{-1} \;&:=\; \mathrm{Toep}\Big\{\ldots, 0, \boxed{0}, \alpha\,A_{-1}, 0, \ldots\Big\} \end{aligned}$$

At any wavenumber pair $\mathbf{k}$, a discretization of the linearized NS equations together with a truncation of the bi-infinite operator-valued matrices would require solving a large-scale generalized Lyapunov equation. We follow [7] in considering small-amplitude oscillations α and utilizing a perturbation analysis to achieve computational efficiency in obtaining the energy spectrum. This choice is also motivated by the observation that large-amplitude oscillations can become prohibitively expensive to generate and result in a negative net efficiency for our flow control strategy [5], [7].

B. Perturbation analysis

Following [20], the solution to (18) can be efficiently computed using a perturbation analysis in α. Specifically, the operator $\bar{\mathcal{F}}$ in (18) can be decomposed into a block diagonal operator $\bar{\mathcal{F}}_0$ and an operator $\bar{\mathcal{F}}_1$ that contains the first upper and lower block sub-diagonals

$$\begin{aligned} \bar{\mathcal{F}} \;&=\; \bar{\mathcal{F}}_0 \;+\; \alpha\,\bar{\mathcal{F}}_1 \qquad (19)\\ \bar{\mathcal{F}}_0 \;&=\; \mathrm{diag}\left\{A_0 - \mathrm{i}\,n\,\omega_t I\right\} \\ \bar{\mathcal{F}}_1 \;&=\; \mathrm{Toep}\left\{\ldots, 0, (1+\mu_1)A_1, \boxed{0}, (1+\mu_{-1})A_{-1}, 0, \ldots\right\} \end{aligned}$$

Moreover, operators $\mathcal{F}_{\pm1}$ take the block-Toeplitz form

$$\begin{aligned} \mathcal{F}_1 \;&=\; \mathrm{Toep}\left\{\ldots, 0, A_1, \boxed{0}, 0, \ldots\right\} \qquad (20)\\ \mathcal{F}_{-1} \;&=\; \mathrm{Toep}\left\{\ldots, 0, \boxed{0}, A_{-1}, 0, \ldots\right\} \end{aligned}$$

For sufficiently small α, the solution $\mathcal{X}$ of (18) can be expanded using the same perturbation series,

$$\mathcal{X} \;=\; \mathcal{X}_0 \;+\; \alpha\,\mathcal{X}_1 \;+\; \alpha^2\,\mathcal{X}_2 \;+\; \ldots \qquad (21)$$

Substituting (19)-(21) into (18) and collecting powers of α yields

$$\alpha^0\colon\ \bar{\mathcal{F}}_0\,\mathcal{X}_0\,+\,\mathcal{X}_0\,\bar{\mathcal{F}}_0^\dagger\ =\ -B\,\Omega B^\dagger$$

$$\alpha^n\colon\ \bar{\mathcal{F}}_0\,\mathcal{X}_n\,+\,\mathcal{X}_n\,\bar{\mathcal{F}}_0^\dagger\ =\ -\Big(\bar{\mathcal{F}}_1\,\mathcal{X}_{n-1}\,+\,\mathcal{X}_{n-1}\,\bar{\mathcal{F}}_1^\dagger\Big)\\ +\,[\delta(n-1)-1]\sum_{i=\pm1}\sigma_i^2\,\mathcal{F}_i\,\mathcal{X}_{n-2}\,\mathcal{F}_i^\dagger$$

where $\delta(n)$ is the discrete delta function. Given the structures of $\bar{\mathcal{F}}_0$, $\bar{\mathcal{F}}_{\pm1}$, and $\mathcal{F}_{\pm1}$, we can determine the block structure of the self-adjoint operators $\mathcal{X}_i$ in (21) as

$$\mathcal{X}_0\ :=\ \mathrm{Toep}\Big\{\ldots,0,\boxed{X_{0,0}},0,\ldots\Big\}$$

$$\mathcal{X}_1\ :=\ \mathrm{Toep}\Big\{\ldots,0,X_{1,1}^\dagger,\boxed{0},X_{1,1},0,\ldots\Big\}$$

$$\mathcal{X}_2\ :=\ \mathrm{Toep}\Big\{\ldots,0,X_{2,2}^\dagger,0,\boxed{X_{2,0}},0,X_{2,2},0,\ldots\Big\}$$

where the first and second indices of the sub-matrices correspond to the perturbation order and harmonic number, respectively. The structure identified for the auto-correlation operators in conjunction with (15) and (17) results in the following perturbation series for X_0:

$$X_0(\mathbf{k})\ =\ X_{0,0}(\mathbf{k})\,+\,\alpha^2\,X_{2,0}(\mathbf{k})\,+\,O(\alpha^4). \qquad (22)$$

Finally, the operators $X_{0,0}$ and $X_{2,0}$ are obtained by solving the following set of Lyapunov equations

$$A_0\,X_{0,0}\,+\,X_{0,0}\,A_0^\dagger\ =\ -B\,\Omega B^\dagger$$

$$(A_0+\mathrm{i}\omega_t I)\,X_{1,1}\,+\,X_{1,1}\,A_0^\dagger\ =\ -\Big((1+\mu_{-1})\,A_{-1}\,X_{0,0}\\ +(1+\mu_1)\,X_{0,0}\,A_1^\dagger\Big)$$

$$A_0\,X_{2,0}\,+\,X_{2,0}\,A_0^\dagger\ =\ -(1+\mu_1)\,(A_1X_{1,1}+X_{1,1}A_1^\dagger)\\ -(1+\mu_{-1})\,(A_{-1}X_{1,1}+X_{1,1}A_{-1}^\dagger)\\ -\sum_{i=\pm1}\sigma_i^2\,A_i\,X_{0,0}\,A_i^\dagger$$

whose individual size is equal to the size of each block of the bi-infinite generalized Lyapunov equation (18). This harmonic-based decoupling is used for efficient computaiton of the second-order statistics of system (8). Finally, the energy spectrum of velocity fluctuations (Eq. (16)) follows a similar perturbation series as (22):

$$E(\mathbf{k})\ =\ E_0(\mathbf{k})\,+\,\alpha^2E_2(\mathbf{k})\,+\,O(\alpha^4) \qquad (23)$$

where $E_0(\mathbf{k})=\mathrm{trace}(X_{0,0}(\mathbf{k}))$ is the energy spectrum in the absence of control, and $E_2(\mathbf{k})=\mathrm{trace}(X_{2,0}(\mathbf{k}))$ captures the effect of boundary control at the level of α^2.

V. Channel flow with random wall oscillations

We study the influence of parametric uncertainty on the MSS and variance of velocity fluctuations in channel flow with $R=2000$ over transverse wall oscillations. We employ a pseudospectral scheme with Chebyshev polynomials [31] to discretize the wall-normal dimension and obtain finite-dimensional approximations of the differential operators in the linearized NS dynamics. Mean-square stability and variance amplification are analyzed for the special case of streamwise-constant velocity fluctuations ($k_x=0$) that are energetically dominant in the absence of control [8]–[10].

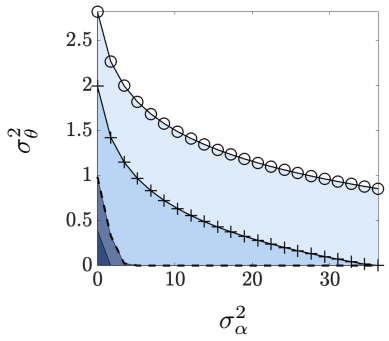

Fig. 3. Stability curves for the dynamics of fluctuations in a channel flow with $R=2000$ and $\mathbf{k}=(0,2)$ subject to random lower-wall oscillations with nominal parameters: $\alpha=0.01$ and $\omega_t=8.8\times10^{-3}$ ($\circ$); $\alpha=0.01$ and $\omega_t=5\times10^{-4}$ ($+$); $\alpha=0.1$ and $\omega_t=8.8\times10^{-3}$ ($--$); $\alpha=0.1$ and $\omega_t=5\times10^{-4}$ (—).

A. MSS in channel channel flow with $(k_x,k_z)=(0,2)$

In the absence of control, the energy spectrum of velocity fluctuations in channel flow with $R=2000$ can be shown to peak at $k_x=0$ and $k_z\approx1.78$, see, e.g., [10]. For $(k_x,k_z)=(0,2)$ and various nominal wall oscillation parameters (α and ω_t), we evaluate the MSS of the controlled flow dynamics in the presence of zero-mean parametric uncertainties γ_α and γ_θ. We note that the first MSS condition, i.e., $\bar{A}$ is Hurwitz, is satisfied no matter the uncertainty level. However, the second condition can be violated as the variances of zero-mean parametric uncertainties γ_α and γ_θ grow. Figure 3 shows the regions of MSS in the presence of such uncertainties. It is evident that stability properties of the channel are more susceptible to parametric uncertainty entering in the phase of wall oscillations and that nominally larger oscillation amplitudes and periods are less robust.

B. Variance amplification

We now study the effect of parametric uncertainties on the performance of our flow control strategy in reducing the energy of velocity fluctuations. We consider the case of lower-wall spanwise wall oscillations with $\alpha=0.01$ and $\omega_t=8.8\times10^{-3}$ that are contaminated with zero-mean parametric uncertainties γ_α and γ_θ of variance 0.06 and 0.2, respectively. Note that at this low level of uncertainty the linear dynamics remain mean-square stable (cf. Fig. 3). Given zero-mean uncertainties with instantaneous normal distributions, such variances ensure that the sources of uncertainty γ_α and γ_θ predominantly reside in the ranges $[-0.5,0.5]$ and $[-\pi/2,\pi/2]$, respectively.

Figure 4 shows the effect of lower-wall spanwise oscillations on the energy of streamwise-constant fluctuations at the level of α^2 (E_2 in Eq. (23)). Results from the perturbation analysis of Section IV-B show that relative to the nominal curve (black solid line) uncertainty in the oscillation amplitude (γ_α) has a negative (albeit relatively small) effect on performance and that uncertainty in the phase (γ_θ) has a positive effect on performance, i.e., it can increase variance

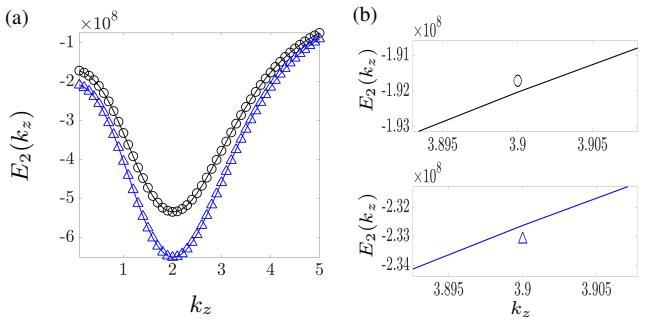

Fig. 4. (a) Energy suppression in streamwise-constant fluctuations due to lower-wall oscillations with $\omega_t = 8.8 \times 10^{-3}$ at the level of α^2 ($E_2(k_z)$) in the absence (solid black line) and presence of zero-mean parametric uncertainty: $\gamma_\alpha = 0$ and $\sigma_\theta^2 = 0.2$ (blue triangles); $\sigma_\alpha^2 = 0.06$ and $\gamma_\theta = 0$ (black circles); $\sigma_\alpha^2 = 0.06$ and $\sigma_\theta^2 = 0.2$ (solid blue line). (b) Magnified views of $E_2(k_z)$ capture the variations caused by uncertainty γ_α.

attenuation. Moreover, the parametric uncertainties maintain the significance of $k_z \approx 2$ as the spanwise wavenumber associated with the largest energy suppression. The dominant influence of γ_θ roots in the dependence of the mean drift $\mu_{\pm 1}$ on σ_θ^2, which directly affects the nominal dynamics $\bar{A}$ (Eq. (10)) and enters as a coefficient to the right-hand-side of the Lyapunov equations of Section IV-B. Our results demonstrate that random phase distortion can indeed improve the ability of small-amplitude wall oscillations to attenuate the energy of velocity fluctuations in channel flows.

VI. Concluding Remarks

We have shown that stochastic parametric imperfections in the amplitude and phase of wall oscillations have the potential to change the dynamical properties of the linearized equations and thereby influence MSS of velocity fluctuations and the performance of this flow control strategy. We have adopted an input-output approach to characterize the frequency response of the channel flow subject to uncertain wall oscillations and provided conditions for MSS. Our analysis shows that despite a clear dependence on the nominal amplitude and frequency of oscillations, velocity fluctuations remain mean-square stable for relatively high levels of uncertainty, which is in agreement with parametric studies on the effect of oscillation amplitude, e.g., [6]. Moreover, our analysis shows that introducing random distortions to the phase of lower-wall oscillations results in a notable increase in energy suppression. Our approach paves the way for the robustness analysis of other control strategies that modify the base state and are prone to parametric uncertainties.

References

[1] K.-S. Choi, "Near-wall structure of turbulent boundary layer with spanwise-wall oscillation," *Phys. Fluids*, vol. 14, no. 7, pp. 2530–2542, 2002.

[2] P. Ricco, "Modification of near-wall turbulence due to spanwise wall oscillations," *J. Turbul.*, vol. 5, pp. 20–20, 2004.

[3] W. Jung, N. Mangiavacchi, and R. Akhavan, "Suppression of turbulence in wall-bounded flows by high-frequency spanwise oscillations," *Phys. Fluids A*, vol. 4, no. 8, pp. 1605–1607, 1992.

[4] M. Quadrio and P. Ricco, "Critical assessment of turbulent drag reduction through spanwise wall oscillations," *J. Fluid Mech.*, vol. 521, pp. 251–271, 2004.

[5] P. Ricco and M. Quadrio, "Wall-oscillation conditions for drag reduction in turbulent channel flow," *International Journal of Heat and Fluid Flow*, vol. 29, no. 4, pp. 891–902, 2008.

[6] M. R. Jovanovic, "Turbulence suppression in channel flows by small amplitude transverse wall oscillations," *Phys. Fluids*, vol. 20, no. 1, p. 014101 (11 pages), January 2008.

[7] R. Moarref and M. R. Jovanovic, "Model-based design of transverse wall oscillations for turbulent drag reduction," *J. Fluid Mech.*, vol. 707, pp. 205–240, September 2012.

[8] B. F. Farrell and P. J. Ioannou, "Stochastic forcing of the linearized Navier-Stokes equations," *Phys. Fluids A*, vol. 5, no. 11, pp. 2600–2609, 1993.

[9] B. Bamieh and M. Dahleh, "Energy amplification in channel flows with stochastic excitation," *Phys. Fluids*, vol. 13, no. 11, pp. 3258–3269, 2001.

[10] M. R. Jovanovic and B. Bamieh, "Componentwise energy amplification in channel flows," *J. Fluid Mech.*, vol. 534, pp. 145–183, July 2005.

[11] W. Ran, A. Zare, M. J. P. Hack, and M. R. Jovanovic, "Stochastic receptivity analysis of boundary layer flow," *Phys. Rev. Fluids*, vol. 4, no. 9, p. 093901 (28 pages), September 2019.

[12] Y. Hwang and C. Cossu, "Linear non-normal energy amplification of harmonic and stochastic forcing in the turbulent channel flow," *J. Fluid Mech.*, vol. 664, pp. 51–73, 2010.

[13] A. Zare, M. R. Jovanovic, and T. T. Georgiou, "Completion of partially known turbulent flow statistics," in *Proceedings of the 2014 American Control Conference*, 2014, pp. 1680–1685.

[14] A. Zare, M. R. Jovanovic, and T. T. Georgiou, "Colour of turbulence," *J. Fluid Mech.*, vol. 812, pp. 636–680, February 2017.

[15] A. Zare, T. T. Georgiou, and M. R. Jovanovic, "Stochastic dynamical modeling of turbulent flows," *Annu. Rev. Control Robot. Auton. Syst.*, vol. 3, pp. 195–219, May 2020.

[16] R. Moarref and M. R. Jovanovic, "Controlling the onset of turbulence by streamwise traveling waves. part 1: Receptivity analysis," *J. Fluid Mech.*, vol. 663, pp. 70–99, November 2010.

[17] W. Ran, A. Zare, and M. R. Jovanović, "Model-based design of riblets for turbulent drag reduction," *J. Fluid Mech.*, vol. 906, p. A7 (38 pages), January 2021.

[18] S. Skogestad and I. Postlethwaite, *Multivariable feedback control: analysis and design*. Wiley New York, 2007, vol. 2.

[19] J. Zhou, T. Hagiwara, and M. Araki, "Trace formula of linear continuous-time periodic systems via the harmonic Lyapunov equation," *Int. J. Control*, vol. 76, no. 5, pp. 488–500, 2003.

[20] M. R. Jovanovic and M. Fardad, "$\mathcal{H}_2$ norm of linear time-periodic systems: a perturbation analysis," *Automatica*, vol. 44, no. 8, pp. 2090–2098, August 2008.

[21] M. Filo and B. Bamieh, "An input-output approach to structured stochastic uncertainty in continuous time," *arXiv preprint arXiv:1806.09091*, 2018.

[22] D. Kleinman, "On the stability of linear stochastic systems," *IEEE Trans. Automat. Control*, vol. 14, no. 4, pp. 429–430, 1969.

[23] D. B. Hewawaduge and A. Zare, "Input-output analysis of stochastic base flow uncertainty," *Phys. Rev. Fluids*, 2020, submitted; also arXiv:2012.14918.

[24] I. Ito, "On the existence and uniqueness of solutions of stochastic integral equations of the Volterra type," *Kodai Mathematical Journal*, vol. 2, no. 2, pp. 158–170, 1979.

[25] R. L. Stratonovich, "A new representation for stochastic integrals and equations," *SIAM J. Control*, vol. 4, no. 2, pp. 362–371, 1966.

[26] B. Øksendal, "Stochastic differential equations," in *Stochastic differential equations*. Springer, 2003, pp. 65–84.

[27] H. J. Kushner, *Stochastic stability and control*. Academic Press, New York, 1967.

[28] J. Willems, "The circle criterion and quadratic Lyapunov functions for stability analysis," *IEEE Trans. Automat. Control*, vol. 18, no. 2, pp. 184–184, 1973.

[29] J. Samuels, "On the mean square stability of random linear systems," *IRE Trans. Circuit Theory*, vol. 6, no. 5, pp. 248–259, 1959.

[30] W. Gardner, *Introduction to Random Processes: with Applications to Signals and Systems*. McGraw-Hill, 1990.

[31] J. A. C. Weideman and S. C. Reddy, "A MATLAB differentiation matrix suite," *ACM Trans. Math. Software*, vol. 26, no. 4, pp. 465–519, December 2000.